

Development of an Impedance Monitoring System for Rechargeable Lithium Batteries

Jorge Miguel Carmo Lourenço
jorge.m.lourenco@tecnico.ulisboa.pt

Instituto Superior Técnico, Lisboa, Portugal

December 2024

Abstract

Due to the excellent energy and power density of lithium-ion batteries compared to other alternatives, the study of their characteristics has become increasingly relevant. The state-of-charge and state-of-health of batteries are closely related to their impedance, which can provide valuable information about their performance and longevity. This work presents the design, testing, and validation of an embedded system capable of performing impedance measurements using the Electrochemical Impedance Spectroscopy method on lithium-ion batteries. The system generates a multiharmonic stimulus that contains frequencies covering a range between 50 mHz and 1 kHz, at which the battery impedance is measured. The Goertzel algorithm is used to calculate the frequency components of the voltage and current signals, given that Coherent sampling is assured. This architecture reduces memory requirements as the samples are discarded after processing. A lithium-ion battery is subjected to multiple impedance measurements at different states of charge and health, allowing for a complete characterization of its operation. Based on the obtained data, an equivalent electrical model is used to accurately describe the tested cell. The parameters of this model are correlated with variations in state-of-charge and state-of-health, providing a platform for future implementation of algorithms to estimate such states, based on impedance measurements.

Keywords: Electrochemical Impedance Spectroscopy, Lithium-Ion Battery, Rechargeable Batteries, State-of-Charge, State-of-Health, Equivalent Circuit Model

1. Introduction

Since first commercialized by Sony Corporation in 1991 [10], Lithium-Ion Batteries (LIBs) have gained notorious popularity across various technological fields. Factors such as low self-discharge rate, no memory effect, high energy density and excellent cycling performance, helped propel LIBs as the cornerstone of energy storage solutions [11], [19].

In practical applications, LIBs are not deployed as a standalone device and are always paired with a Battery Management System (BMS). A BMS consists of hardware and software capable of online: voltage, temperature and current monitoring of battery cell/s to ensure safe operation within battery limits. In addition, since batteries are complex electrochemical devices with a distinct nonlinear behavior depending on various internal and external conditions, special algorithms for battery monitoring are required [16], [8]. Online algorithms for State-of-Charge (SoC) and State-of-Health (SoH) play a pivotal role due to their direct reflection of overall battery performance [3]. In general, $SoC(t)$ is defined as the ratio between the current cell ca-

capacity, $Q(t)$, and the maximum cell capacity at a given state of aging, Q_{max} , [3], typically displayed as a percentage

$$SoC(t) = \frac{Q(t)}{Q_{max}} \cdot 100\% \quad [\%]. \quad (1)$$

The SoH has been defined in the literature as

$$SoH = \frac{Q_{max}}{Q_n} \cdot 100\% \quad [\%], \quad (2)$$

where Q_n is the nominal capacity of the battery, stated in the manufacturer datasheet. It is considered that the battery has reached its end of life when SoH reaches around 80 % [18], [9]. To compute a SoH estimation, means, finding Q_{max} , given that Q_n is a fixed value. The accurate and robust determination of these states is crucial, as it enables the implementation of smart control strategies for energy management. These strategies bring valuable benefits, including the potential to significantly extend the overall lifespan of the battery, reducing maintenance cost, which is extremely valuable in the case of large battery packs as is the case in electric vehicles.

Since it is not possible to directly measure the chemical energy stored in a battery [19], estimating SoC and SoH becomes a complex task, often requiring significant computational power and extensive test data. Indirect estimation relies on measured battery variables, such as voltage, current, and temperature, processed through mathematical models [3], [17]. This task is additionally hindered by considerable changes in battery characteristics over its lifetime due to aging [15].

2. Electrochemical Impedance Spectroscopy

Electrochemical Impedance Spectroscopy (EIS) [2] is a powerful measurement technique, particularly useful for characterizing the behavior of interfaces, such as electrodes and electrolytes in batteries. The technique provides insights into processes such as charge transfer reactions, diffusion, and other electrochemical phenomena, making it a versatile and non-invasive tool for characterisation of LIBs. EIS data, may be used to analyze and estimate several crucial parameters that describe the condition of a battery, including the SoC and the SoH, potentially solving the problems that conventional estimation methods face.

The method works by applying a small amplitude periodic perturbation either current, Galvanostatic Electrochemical Impedance Spectroscopy (GEIS) or voltage, Potentiostatic Electrochemical Impedance Spectroscopy (PEIS), to the system being studied. The system's reaction to the applied perturbation, whether in current, GEIS, or voltage, PEIS, is measured and recorded as a transfer function. This response is then processed to derive the system impedance.

The perturbation signal, also referred as excitation signal, in the most basic EIS setup, is a single-tone sinusoidal signal. In GEIS, current is used for the excitation signal, and it is stated in function of time as

$$i(t) = I_0 \cdot \cos(\omega \cdot t + \phi_I) \quad [\text{A}], \quad (3)$$

where (I_0) is the signal's amplitude, (ω) angular frequency and (ϕ_I) current phase. The system's reaction, voltage signal, is

$$u(t) = U_0 \cdot \cos(\omega \cdot t + \phi_V) \quad [\text{V}], \quad (4)$$

where (U_0) is the signal's amplitude and (ϕ_V) the voltage phase. Impedance (Z) is a measurement of opposition to an alternating flow of current within an electric circuit, expressed in (Ω). With Euler's relationship, it is possible to express both voltage and current signal as phasors

$$\bar{I} = I_0 \cdot e^{(j\phi_I)} \quad [\text{A}], \quad (5)$$

$$\bar{U} = U_0 \cdot e^{(j\phi_V)} \quad [\text{V}]. \quad (6)$$

Impedance is defined as the ratio between the voltage and current phasors

$$Z = \frac{\bar{U}}{\bar{I}} = \frac{U_0}{I_0} \cdot e^{(j(\phi_V - \phi_I))} = Z_0 \cdot e^{(j\cdot\phi_Z)} \quad [\Omega]. \quad (7)$$

Impedance can be presented in Cartesian form, $Z = R + jX$, where the real part of the impedance is the resistance (R) and the magnitude of the imaginary part is the reactance (X),

$$R = Z_0 \cdot \cos(\phi_Z) \quad [\Omega], \quad (8)$$

$$X = Z_0 \cdot \sin(\phi_Z) \quad [\Omega]. \quad (9)$$

This process is measured across a range of frequencies, typically in the mili-Hertz (mHz) to kilo-Hertz (kHz) range, thereby generating a characteristic impedance spectrum.

2.1. Excitation signal design

Broadband multi-sine signals as a source of excitation for EIS systems provide simultaneous measuring results at all interest frequencies, thus, considerably reducing the testing time needed to obtain an EIS spectrum curve [5].

The signal designed consists on the sum of 15 sinusoidal components with a quasi-logarithmic spacing, as in most EIS systems [5], [1], [6]. The selected values of the excited frequencies are: 0.05, 0.1, 0.2, 0.4, 1, 2, 4, 10, 20, 40, 80, 160, 320, 640, 1000 Hz. The signal is

$$x(t) = \sum_{k=1}^{15} \cos(\omega_k t + \phi_k), \quad (10)$$

where $\omega_k = 2\pi f$ rad/s and ϕ_k are the phase for each component, which need to be carefully selected to minimize the signal's Crest Factor (CF).

All frequencies are integer multiples of the first. This ensures that the data recordings contains integer periods of each sinusoidal component. This enables the elimination of spectral leakage in computation of the Discrete Fourier Transform (DFT) according to [1].

The phase of each sine wave plays a pivotal role in the design of the signal. Typically, phases are randomly assigned, Figure 1, but generally this approach produces high peak values of the waveform [13], which is usually characterized by the CF, defined as the ratio between the modulus of signal's peak value ($|x_{pk}|$) and Root Mean Square (RMS) (x_{RMS})

$$CF = \frac{|x_{pk}|}{x_{RMS}}. \quad (11)$$

A sinusoidal signal has by definition a CF of 1.414. For broadband multi-sine signals a CF between 1.8 and 2.5 is acceptable. This is of extreme

importance given that, the lower the CF the higher the Signal-to-Noise Ratio (SNR) of the excitation signal, which ultimately provides higher accuracy for EIS measurements [13]. The correct combination of phases that minimize the CF for a multi-sine signal has been an open mathematical problem for the last 5 decades [13]. The Clipping Algorithm is used for minimization of the signal’s CF. It operates as an iterative process starting with randomly assigned phase values for each frequency bin. After generating the initial time-domain signal from the first set of phases, the following steps are executed: computing the signal’s CF, clipping the time-domain signal such that its amplitude is limited to a specified percentage of the current absolute peak value, determining the DFT of the resulting signal, restoring the amplitudes to the initial desired values while keeping the phases from the DFT result, and if the CF reaches a desirable value or there is no significant improvement, the algorithm is stopped. Otherwise, a new time-domain signal is computed from the new set of phases, and the process is repeated with a new clipping percentage which is gradually increased over the iterations from 75 % to 99 %.

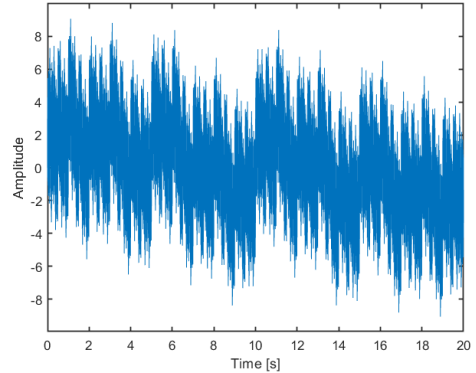
Figure 2 illustrates the resulting excitation signal after CF optimization. The final CF is 2.139 which is within reasonable limits for a multisine broadband signal with 15 frequency bins.

To respect the Nyquist-Shannon sampling theorem the sampling frequency should be at least twice the highest frequency component, $FS_{min} = 2 \cdot 1000 = 2 \text{ kHz}$. A sampling rate of 10 kSa/s allows for a resolution of 10 samples per period for the highest frequency component while keeping the memory requirements to store the excitation signal reasonable. The multi-sine period is 20 s, which corresponds to the period of the lowest frequency component, 0.05 Hz.

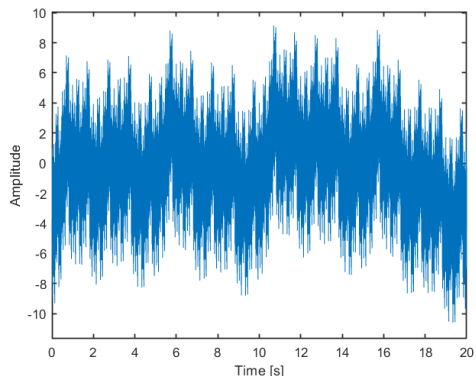
Higher amplitude of the excitation signal shows to improve the SNR [5]. For this work, an amplitude of 50 mA will be used as a baseline, motivated by [5].

3. Embedded System Overview

The system design has three key features: 1. EIS measurements tailored for LIB technology. 2. Capability to characterize a LIB using EIS across different temperatures, charge levels, and life cycles to develop accurate SoC and SoH estimation methods. 3. Possible platform for future implementation of two methods for accurate on-line estimations of SoC and SoH when connected to any LIB. See Figure 3 for proposed system’s architecture.



(a)



(b)

Figure 1: Broadband signal without Crest Factor optimization: (a) Phases set to zero; (b) Phases assigned randomly.

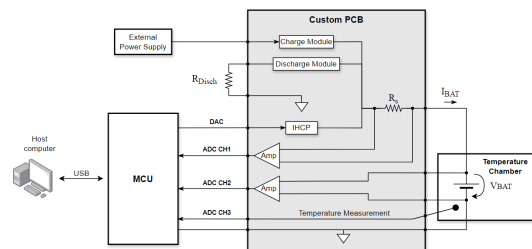


Figure 3: Proposed system’s architecture overview.

A four-wire (or Kelvin) connection is implemented to connect the system to the battery under test. In order to consider different ambient temperature conditions, the battery will be placed in a controlled temperature, model Pentalab EF-3.

A custom Printed Circuit Board (PCB) with essential analog circuitry is designed for increased flexibility and compactness, tailored specifically for this work. It includes circuitry for EIS measurements, a shunt current measurement for its popularity in EIS setups, and an Improved Howland Current Pump (IHCP) circuit for excitation signal

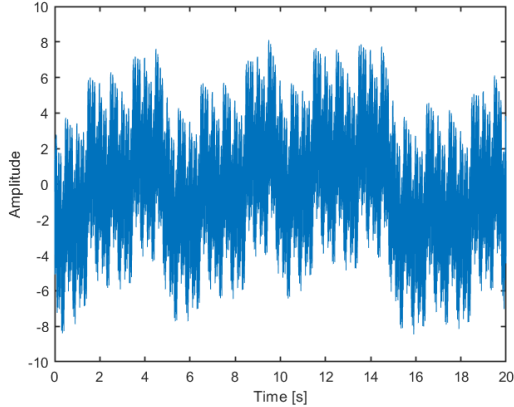


Figure 2: Signal after Crest Factor optimization.

sourcing. The PCB has separate charge and discharge circuits for a 3 A maximum current, equivalent to a 1 C rate for a 3 Ah battery, balancing characterization time and compactness. Increasing the rate would require more expensive components and added complexity. It also contains a temperature sensor with measuring range 0° C, to 60° C. The board was developed using Altium Designer and comprises of a single module measuring 86 mm by 108 mm, with two 35 μ m layers and a board thickness of 1.6 mm, as shown in Figure 4.

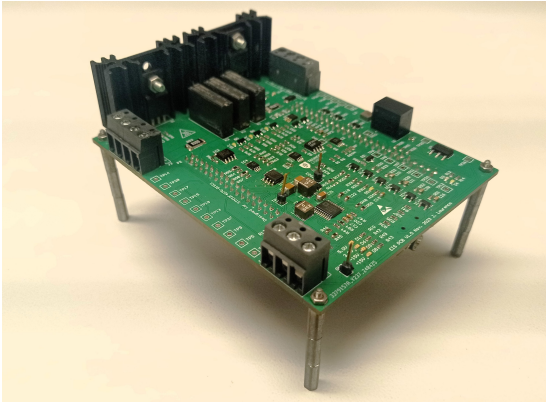


Figure 4: Fully assembled PCB.

3.1. Micro Controller Unit

The STM32F407G-DISC1 prototype board is used for computational power. It boasts a high-performance ARM Cortex-M4 processor with a clock speed of up to 168 MHz. It offers a comprehensive set of peripherals and interfaces, including 16 12-bit Analog to Digital Converter (ADC) channels, two Digital to Analog converter (DAC) outputs with Direct Memory Access (DMA), 1 MB of flash memory and a Universal Serial Bus (USB) interface. Micro Controller Unit (MCU)s from the same family have been used in several experimental

setups for battery states estimation and EIS instrumentation [21], [20], [12], [4].

3.2. Excitation signal source

The EIS excitation signal is sourced by an IHCP circuit. The selected amplifier is a LT1217 from Linear Technology with maximum output current of 100 mA. The IHCP is a circuit designed to amplify a differential voltage in order to impose a current across a fixed shunt resistor. This creates a voltage controlled current source non-dependent on the voltage developed by the load, (V_{load}). Figure 5 presents the basic schematic for an IHCP.

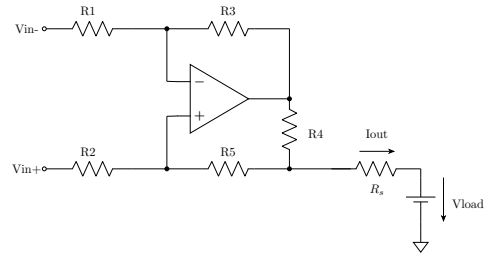


Figure 5: Improved Howland Current Pump Circuit.

The desired output current I_{out} is ± 50 mA for a control voltage of ± 5 V

$$I_{out} = \frac{G \cdot (V_{in+} - V_{in-})}{R_4} \quad [A], \quad (12)$$

$$G = \frac{R_3}{R_1}, \quad \frac{R_3}{R_1} = \frac{R_5 + R_4}{R_3} \quad [V/V]. \quad (13)$$

Resistors R_3 and R_1 are therefore set to 1 k Ω , R_4 to 100 Ω and R_5 to 898 Ω . The control signal is sourced by a dedicated DAC output which features DMA for quick sampling of the excitation signal directly from memory.

The STM32 DAC outputs a voltage between 0 V to 3.3 V. In order to convert the signal to ± 5 V a differential amplifier circuit, is used to convert the DAC output to a bipolar voltage centered at 0 V. This is achieved by subtracting the DAC output by half the DAC range, 1.65 V respectively.

3.3. Current measurement

Two different scenarios are considered for current measurement. One when an EIS measurement is being performed, ± 50 mA, the other when the cell is being discharged/charged, ± 3 A.

The current output to the test battery flows through a 100 m Ω shunt resistor, R_s . The voltage differential across the resistor terminals is amplified by an Instrumentation Amplifier (IA), AD620, with $G \approx 39$, to also have a single-ended output referenced to ground. After amplification by the IA for the EIS measurements the voltage signal is between $\pm 5 \text{ mV} \cdot 39 = \pm 195 \text{ mV}$ and for

charge/discharge mode is $\pm 0.3 \text{ V} \cdot 39 = \pm 11.7 \text{ V}$. Given that the STM32 ADC is rated for inputs between $[0 \text{ V} - 3.3 \text{ V}]$, there is the need for increased amplification of the signal for the EIS measurements and attenuation of the signal for the charge/discharge. Two similar circuits are design, using a non-inverting summing amplifier circuit. The idea is to sum the output of the IA, current measurement, subjected to a gain, with 1.65 V , half the range of the STM32 ADC in order to achieve a unipolar signal which takes advantage of most of the ADC range.

To protect the ADC inputs, a series resistor with two anti-parallel schottky diodes is used to limit the output to normal voltage levels for both measuring circuits.

Figure 6 shows the complete current measurement circuit.

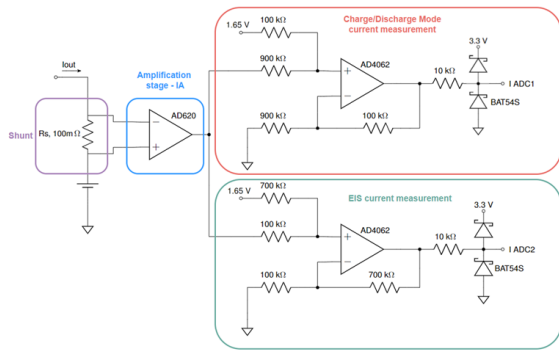


Figure 6: Current measurement circuit overview.

3.4. Voltage measurement

When performing an EIS measurement, the battery voltage will consist of a DC component plus an AC response to the applied current perturbation

$$V_{BAT}(t) = V_{DC} + V_{AC}(t) \quad [\text{V}]. \quad (14)$$

To measure the response to the applied EIS perturbation, V_{AC} , it is essential to disregard the Direct Current (DC) component, V_{DC} . This is achieved by first sampling V_{BAT} multiple times when no EIS measurement is active, providing an estimate of V_{DC} . This estimated V_{DC} is then fed back into the circuit to be subtracted from the original signal, isolating the Alternating Current (AC) response, see Figure 7. Two Pulse Width Modulation (PWM) outputs which are filtered to produce a constant voltage are summed. PWM2 contributes with a voltage between 0 V and 4.579 V with a 45.79 mV resolution while PWM1 contributes with a voltage between 0 mV and 45.79 mV with $457.9 \mu\text{V}$ resolution.

A differential amplifier circuit is used to subtract V_{DC} , sourced by the circuit depicted in Figure 7,

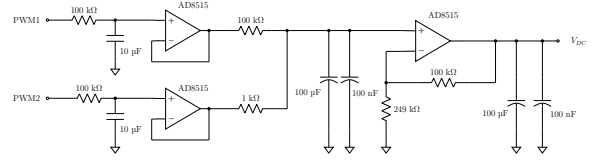


Figure 7: Circuit for generating the DC component of the measured battery voltage.

from V_{BAT} , output of the IA. The gain for this circuit was set to 200 for the first experimental trials and latter on changed to 140. The final stage consists of a non-inverting summing amplifier circuit to convert the bipolar V_{AC} signal to unipolar by centering it around 1.65 V , similar to the circuit used in Figure 6.

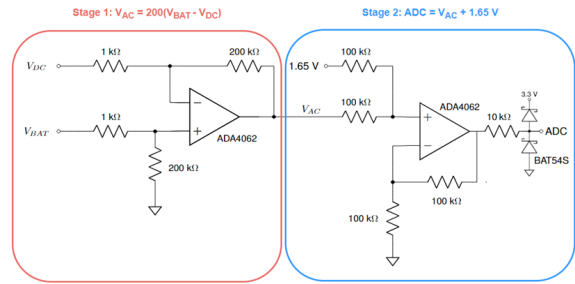


Figure 8: Battery voltage response, V_{AC} , measurement schematic.

3.5. Goertzel Algorithm

In this project, the Goertzel algorithm is used, because it can target a specific frequency bin f_k on the DFT for EIS voltage and current. The algorithm evaluation is performed at the fifteen frequency bins constituting the multisine broadband signal used for EIS injection. The algorithm is more numerically efficient when working with a small number of selected frequency bins compared to the DFT, [14], which makes it particularly well-suited for embedded applications, as is the case with this work. To ensure accurate measurement results with the Goertzel algorithm, it is essential to maintain coherence of the measured signal. Spectral leakage happens when energy from a specific frequency spreads into adjacent frequencies, distorting the results. Coherence allows the algorithm to focus on the desired frequency components, thereby reducing the risk of leakage.

4. Results

EIS measurements are performed in a controlled laboratory setup. The cell is placed inside the temperature chamber model Pentlab EF-3 with a set-point of 25° C .

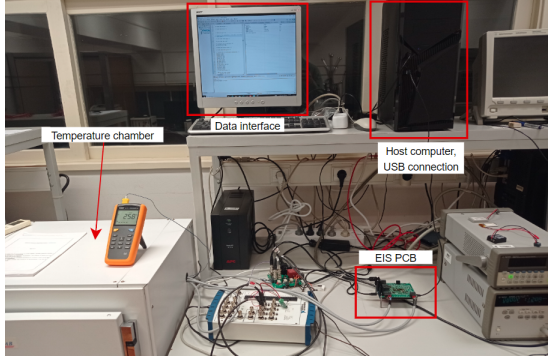


Figure 9: Laboratory setup for EIS measurements.

4.1. Calibration

Calibration for the voltage and current measurements is done using a reference measurement from a laboratory multimeter, model HP 34401A. These are essential for accurate impedance calculations. Subsequently, a commercial impedance measurement device (a Hioki 3522-50 LCR meter) and a test resistor of 100 mΩ are used to establish a baseline for comparison between the measurements of the developed system and those of the Hioki impedance reference instrument. See Figure 10 for calibration results obtained for the 100 mΩ calibration resistor.

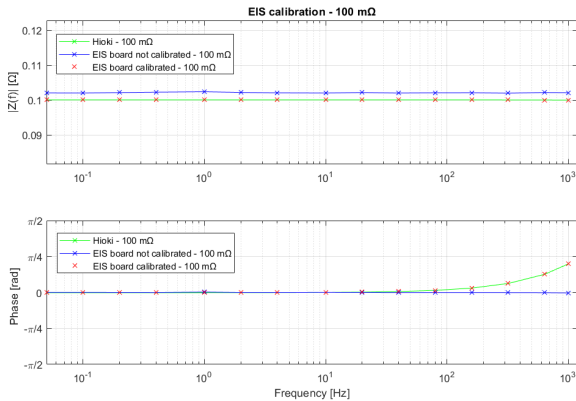


Figure 10: Comparison of EIS measurements from calibration resistor.

4.2. Test battery

The battery used for the impedance measurements is a CELLEVIA BATTERIES L502248 450 mAh Lithium-Polymer (LiPo) cell. The battery includes a protection circuit to avoid over-discharge and over-charge.

4.3. Procedure

Between EIS measurements the cell is cycled 10 times. The charge current is set to 500 mA (1.1 C) and the discharge resistor is 10 Ω, which gives a current between 420 mA and 250 mA (0.93 C - 0.55 C). End of discharge is reached when

battery voltage goes below 2.5 V and end of charge is reached when the charge current goes below 20 mA. full cycle takes approximately 4 hours to finish, see Figure 11.

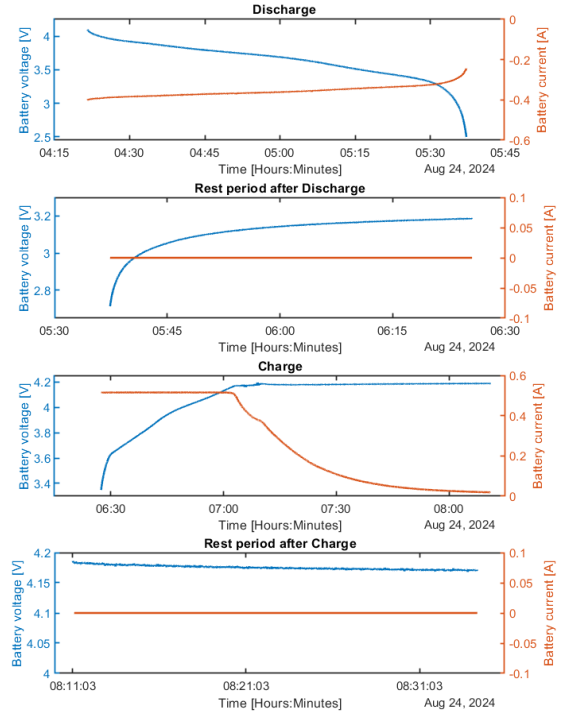


Figure 11: Overview of the different stages during a full charge/discharge cycle.

Each set of EIS measurements includes data collected at increments from 10 % to 100 % of SoC spaced by 10 %. The capacity corresponding to 100 % SoC, Q_{max} , is updated as the most recent recorded capacity after a complete charge cycle, as this provides the most accurate estimate of the battery's true capacity following an EIS test. If the test is being conducted for the first time on a new battery, a manual charge and discharge cycle is performed beforehand to establish an initial capacity reference.

The process begins with the battery fully discharged, and the Coulomb counter reset to 0 Ah. The battery is then charged until the cumulative charge, measured by Coulomb counting, reaches each successive 10 % increment relative to the initial estimated maximum capacity, Q_{max} . After each increment, the battery rests to achieve a steady-state, after which an EIS measurement is performed, starting with the initial measurement at 10 % SoC. This cycle of charging, resting, and measuring continues until 90 % SoC is reached. Finally, the battery is charged to its end-of-charge condition and a final measurement is taken at 100 % SoC, which completes the measurement series. Since the

final maximum battery capacity is likely different than the pre-stipulated battery maximum capacity Q_{max} , SoC levels between 10 % and 90 % are recalculated after the test ends and the real maximum capacity is determined. A single batch of measurements, for the setup used, takes around 6 hours.

4.4. Measurements

The data presented is from a cell which underwent 55 charge-discharge cycles. In order to extract useful information out of the raw measurements an Equivalent Circuit Model (ECM) was used. The resulting model is illustrated in Figure 12 and aligns with a well-established ECM. While alternative models were evaluated, they exhibited inferior fitting performance compared to the selected model. More complex models risk over-fitting and introduce additional parameters, complicating the feature extraction process.

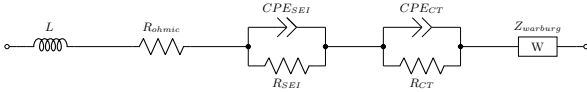


Figure 12: ECM used for EIS data fitting.

The model is established outside the measuring system. The model has 9 parameters, L , R_{ohmic} , R_{SEI} , Q_{SEI} , α_{SEI} , R_{CT} , Q_{CT} , α_{CT} and θ_w .

The model fitting is performed using the least squares curve fitting method. Boundary conditions are set to ensure that the fitted parameters remain within physically meaningful ranges. Parameters α_{CT} and α_{SEI} are bounded between 0 and 1, while for the rest of the parameters a lower bound of 0 is defined. It is important to note that the algorithm provides a solution which is identical by switching the order of the two Constant Phase Elements (CPEs) and corresponding resistor parallel circuit, as the total impedance of the circuit remains the same. For this reason a constrain is set to enforce $R_{SEI} \cdot Q_{SEI} < R_{CT} \cdot Q_{CT}$ so that the parameters corresponding to the Solid Electrolyte Interfaces (SEIs) are associated with higher frequencies compared to the parameters associated with charge transfer reactions as expected. If this condition is not met the values are exchanged and the corresponding values for α and Q are also swapped.

The results are presented in three formats: magnitude (left), phase (center), and Nyquist plot (right), illustrating the variations across different SoC levels within the frequency range used in this work. See Figure 13 for the EIS measurements taken at cycles equal to 55.

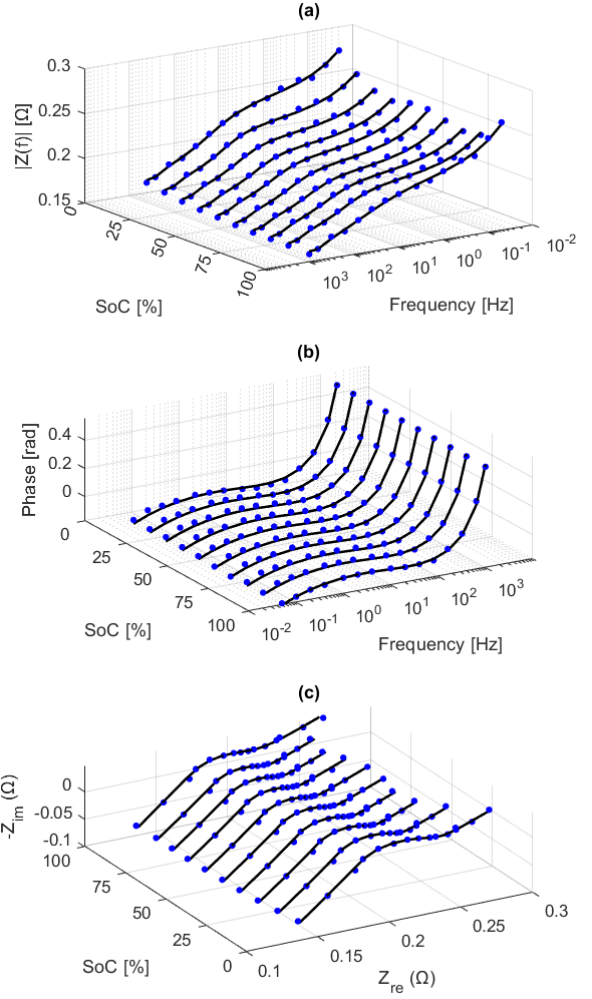


Figure 13: Batch of EIS measurements, at cycles equal to 55: blue (Original measurement); black (ECM). Z_{re} - Real part of Impedance, Z_{im} - Imaginary part of Impedance.

Several adjustments were made during the testing phase. Four distinct batches of measurements were obtained, each associated with different testing conditions, as a reaction to necessary changes in the hardware or testing parameters. The results from the fourth batch showed improved and more consistent measurements, enabling the extraction of usable ECM parameters and corresponds to a full characterization for the selected cell model. For this measurement batch only 5 cycles were performed in between measurements due to time constraints.

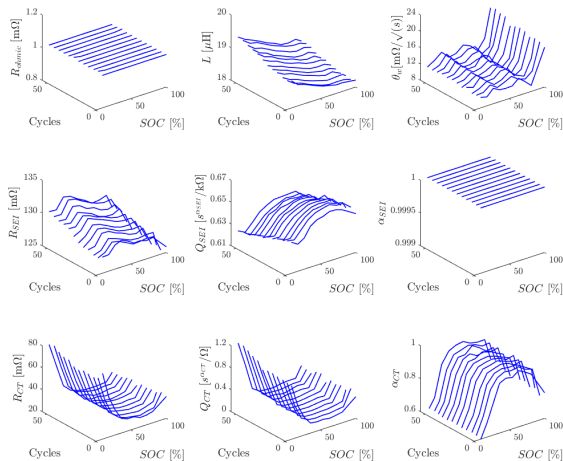


Figure 14: Comparison of ECM parameters for different SoC as the battery ages through charge/discharge cycles.

In Figure 14 the obtained ECM parameters are presented, which show the parameters evolution with SoC, along with the aging of the cell as the number of discharge/charge cycles increases. Although parameter R_{CT} shows a remarkable increase when SoC lowers, that does not occur at SoC values close to 100 %. However, at higher SoC values the Warburg element parameter, θ_w , also increases.

As the number of cycles increases (i.e., the cell ages) the resistance of the SEI increases for all SoC, while Q_{SEI} decreases. The same effect can be found in R_{CT} and Q_{CT} but to a lesser extent.

These findings suggest that, in particular, the evolution of R_{SEI} and Q_{SEI} may serve as a robust indicator of the SoH evolution, while R_{CT} together with θ_w can serve as markers for SoC variations. Additionally, it is worth noting that the parameter α_{SEI} remains constant at 1 throughout the tests, indicating that the CPE behaves as an ideal capacitor. This suggests that modeling the SEI layer with a simpler RC parallel circuit would suffice. Such simplification would simplify the ECM by reducing its total number of parameters from 9 to 8, simplifying the fitting process.

5. Conclusions

The development of an impedance measurement system specifically designed for LIBs has been successfully achieved encompassing the design, testing, and calibration of the system. This system is validated for its ability to accurately measure impedance under a range of SoC and SoH conditions. Additionally, the system allows for thorough battery characterization over variable charge/discharge C-rates, capable of being adapted

for cells with capacities up to 3 Ah. However, in this study, the influence of C-rate on the battery impedance was not performed as a result of the time consuming nature of the measurements also due to battery cycling. This system serves as a versatile framework for expanding battery analysis. The system harnesses the processing power of an STM32F407VGT6 ARM Cortex-M4 MCU, running at a speed of 168 MHz. A DAC channel is employed to drive an IHCP, generating the necessary current stimulus for battery testing. A multisine broadband signal was designed that contained 15 frequency bins, covering a spectrum from 50 mHz to 1 kHz, which aim to capture the different electrochemical phenomena of the test battery, within a brief span of 20 seconds. The Goertzel algorithm is deployed to calculate the frequency components of voltage and current measurements, allowing this to be performed at a sampling frequency of 10 kHz with minimal hardware overhead. The functionality of the Goertzel algorithm is enabled by synchronized excitation and measurement circuits, eliminating spectral leakage.

This system is well suited for laboratory settings without dependence on external components. Its design is compact, but it can be further reduced by integrating the MCU and its relevant circuits in the custom PCB, removing unnecessary peripherals of the existing STM32 development kit. In the future a system without the need for the characterization circuitry, including charge and discharge elements, could reduce the total system size substantially. This would be the case if the prior characterization had already been performed and the system only measures the connected battery impedance and estimates SoC and SoH. This reduction hints at the feasibility of developing a highly compact system that could be seamlessly installed in a wide range of battery applications in the future.

The employment of an ECM facilitated substantial understanding of how different SoC and SoH levels influence impedance measurements. The parameters R_{CT} and θ_w together could provide a marker for SoC estimation while R_{SEI} and Q_{SEI} could be used for SoH estimation. Prospective research could engineer a method to accurately determine SoC and SoH based on the previously mentioned parameters. However, if future tests covering more variables, such as temperature, reveal that it is impractical or too complex to use the ECM parameters for estimation purposes, Machine Learning (ML) methods could be explored to automatically detect relevant characteristics from measured data and the latter could be used for training a Artificial Neural Network (ANN) to estimate SoC and SoH. Despite the encouraging findings, initial EIS measurements indicated an impedance of approx-

imately 110 m Ω at 1 kHz under brand new conditions, in contrast to the manufacturer's new cell impedance of 78 m Ω at 1 kHz. This difference implies that manufacturers might portray overly ambitious specifications, perhaps to enhance battery market appeal by suggesting greater efficiency than is achievable in practice. At the beginning of the project, accurately assessing the battery's performance from its new state across all cycles was difficult due to inconsistencies in EIS measurements. This challenge required various hardware modifications and adjustments to the testing protocols. A C-rate of approximately 1 C was found to be too aggressive, leading to rapid degradation, approximately 2.5 mAh per cycle, which means a loss of 0.5 % capacity per cycle for the selected test battery. This intense cycling increased the polarization effect at both SoC extremes, 0 % and 100 %, gradually increasing the required relaxation time. Deviations in test conditions, particularly longer waiting periods between cycles caused by issues in EIS measurements and loss of power supply, invalidated the early capacity results. Some studies suggest that extending waiting periods to 8 hours or more may improve lithium-ion redistribution within cells [7], potentially leading to more consistent results and providing a greater time margin to address potential problems faced between measurements. However, this approach prolongs the timeline for complete battery characterization and may be substantially different from real world use of the battery.

Acknowledgements

I would like to acknowledge the resources provided by Instituto de Telecomunicações (IT) and Instituto Superior Técnico (IST) that enabled me to conduct this research.

References

- [1] E. Buchicchio, A. De Angelis, F. Santoni, P. Carbone, F. Bianconi, and F. Smeraldi. Dataset on broadband electrochemical impedance spectroscopy of lithium-ion batteries for different values of the state-of-charge. *Data in Brief*, 45:108589, 2022.
- [2] B.-Y. Chang and S.-M. Park. Electrochemical impedance spectroscopy. *Annual Review of Analytical Chemistry*, 3:207–229, 2010.
- [3] W.-Y. Chang. The state of charge estimating methods for battery: A review. *International Scholarly Research Notices*, 2013, 2013.
- [4] G. Cicioni, A. De Angelis, F. M. Janeiro, P. M. Ramos, and P. Carbone. Battery impedance spectroscopy embedded measurement system. *Batteries*, 9(12):577, 2023.
- [5] A. De Angelis, E. Buchicchio, F. Santoni, A. Moschitta, and P. Carbone. Practical broadband measurement of battery eis. In *2021 IEEE International Workshop on Metrology for Automotive (MetroAutomotive)*, pages 25–29. IEEE, 2021.
- [6] A. De Angelis, P. Carbone, A. Moschitta, M. Crescentini, R. Ramilli, P. Traverso, et al. A fast and simple broadband eis measurement system for li-ion batteries. In *24th IMEKO TC4 International Symposium and 22nd International Workshop on ADC and DAC Modelling and Testing*, pages 157–161. International Measurement Confederation (IMEKO), 2020.
- [7] Y. Hu, Y. Yin, and S.-Y. Choe. Accelerated equilibration for lithium-ion battery using optimal time control with electrochemical model. *Journal of Power Sources*, 480:228623, 2020.
- [8] S.-C. Huang, K.-H. Tseng, J.-W. Liang, C.-L. Chang, and M. G. Pecht. An online soc and soh estimation model for lithium-ion batteries. *Energies*, 10(4):512, 2017.
- [9] D. Li, D. Yang, L. Li, L. Wang, and K. Wang. Electrochemical impedance spectroscopy based on the state of health estimation for lithium-ion batteries. *Energies*, 15(18):6665, 2022.
- [10] Y. Liang, C.-Z. Zhao, H. Yuan, Y. Chen, W. Zhang, J.-Q. Huang, D. Yu, Y. Liu, M.-M. Titirici, Y.-L. Chueh, et al. A review of rechargeable batteries for portable electronic devices. *InfoMat*, 1(1):6–32, 2019.
- [11] M. Morris and S. Tosunoglu. Comparison of rechargeable battery technologies. *ASME early career technical journal*, 11:148–155, 2012.
- [12] P. Ningrum, N. A. Windarko, and S. Suhariningsih. Estimation of state of charge (soc) using modified coulomb counting method with open circuit compensation for battery management system (bms). *JAREE (Journal on Advanced Research in Electrical Engineering)*, 5(1), 2021.
- [13] J. Ojarand and M. Min. Recent advances in crest factor minimization of multisine. *Elektronika ir Elektrotechnika*, 23(2):59–62, 2017.
- [14] N. M. Rodrigues, F. M. Janeiro, and P. M. Ramos. Implementation of goertzel-based frequency estimation for power quality monitoring in embedded measurement systems. *Metrology and Measurement Systems*, 29(3), 2022.

- [15] B. Stiaszny, J. C. Ziegler, E. E. Krauß, M. Zhang, J. P. Schmidt, and E. Ivers-Tiffée. Electrochemical characterization and post-mortem analysis of aged $\text{LiNi}_{0.2}\text{Co}_{0.4}\text{Mn}_{0.4}\text{O}_2$ /graphite lithium ion batteries part ii: Calendar aging. *Journal of Power Sources*, 258:61–75, 2014.
- [16] W. Waag, C. Fleischer, and D. U. Sauer. Critical review of the methods for monitoring of lithium-ion batteries in electric and hybrid vehicles. *Journal of Power Sources*, 258:321–339, 2014.
- [17] J. Zhang and J. Lee. A review on prognostics and health monitoring of li-ion battery. *Journal of power sources*, 196(15):6007–6014, 2011.
- [18] M. Zhang, Y. Liu, D. Li, X. Cui, L. Wang, L. Li, and K. Wang. Electrochemical impedance spectroscopy: A new chapter in the fast and accurate estimation of the state of health for lithium-ion batteries. *Energies*, 16(4):1599, 2023.
- [19] Y. Zhang, C. Zhang, and X. Zhang. State-of-charge estimation of the lithium-ion battery system with time-varying parameter for hybrid electric vehicles. *IET Control Theory & Applications*, 8(3):160–167, 2014.
- [20] Z. Zhang, L. Jiang, L. Zhang, and C. Huang. State-of-charge estimation of lithium-ion battery pack by using an adaptive extended kalman filter for electric vehicles. *Journal of Energy Storage*, 37:102457, 2021.
- [21] Z. Zhang, L. Zhang, L. Hu, and C. Huang. Active cell balancing of lithium-ion battery pack based on average state of charge. *International Journal of Energy Research*, 44(4):2535–2548, 2020.